applied optics

Uncertainty in the bidirectional reflectance model for oceanic waters

Peng-Wang Zhai,[1,*] Yongxiang Hu,[2] Charles R. Trepte,[2] David M. Winker,[2] Patricia L. Lucker,[3] Zhongping Lee,[4] and Damien B. Josset[5]

[1]Department of Physics, University of Maryland, Baltimore, Maryland 21250, USA
[2]MS 475 NASA Langley Research Center, Hampton, Virginia 23681-2199, USA
[3]SSAI, MS 475 NASA Langley Research Center, Hampton, Virginia 23681-2199, USA
[4]School for the Environment, University of Massachusetts, Boston, Massachusetts 02125, USA
[5]NRC Research Associate/NRL SSC, 1009 Balch Blvd., Stennis Space Center, Massachusetts 39529, USA
*Corresponding author: pwzhai@umbc.edu

Received 4 February 2015; revised 27 March 2015; accepted 27 March 2015; posted 30 March 2015 (Doc. ID 233902); published 27 April 2015

We study the impacts of the bio-optical model variations on the angular distribution (f/Q factor) of the upwelling radiance field in ocean waters. An ocean water bio-optical model has been combined with a vector radiative transfer model to calculate the f/Q factors systematically. The f/Q factors are compared to those in [Appl. Opt. 41, 6289 (2002)] and the differences are found to be within ±10% for 81% of the total number of cases covering all wavelengths, chlorophyll a concentrations, and solar and viewing geometries. The differences are attributed to the choice of ocean water scattering function and scattering coefficient biases. In addition, we study the uncertainty of f/Q factor due to three factors: (I) the absorption coefficient of the colored dissolved organic matter (CDOM), (II) the particle scattering coefficient, and (III) the ocean water depolarization. The impacts of ocean water depolarization on the f/Q variation is found to be negligible. If we perturb the CDOM absorption coefficient by a factor ranging from 0.1 to 10, the f/Q values vary within ±5% of the average behavior of ocean waters for 93% of the cases. If we perturb the scattering coefficients by a factor ranging from 0.5 to 2.0, the f/Q variation is within ±5% for 81% of the cases studied. This work contributes to understanding the uncertainty of ocean color remote sensing.

OCIS codes: (010.4450) Oceanic optics; (010.4458) Oceanic scattering; (010.5620) Radiative transfer; (290.4210) Multiple scattering; (290.5840) Scattering, molecules; (290.5850) Scattering, particles.

http://dx.doi.org/10.1364/AO.54.004061

1. INTRODUCTION

Ocean color remote sensing is an indispensable way of studying and monitoring the Earth environmental change [1]. The radiance field at the top of the atmosphere includes contributions from both the atmosphere and ocean. In order to extract desirable ocean color information, a procedure called the atmospheric correction is used to remove the atmospheric contribution in operational algorithms of a few major satellite missions [2–12]. Furthermore, the retrieval of total pigments, chlorophyll a [Chl] concentration in milligrams per cubic meter (mg m^{-3}) is achieved by correlating the nadir-viewing water-leaving radiance, or equivalently the remote sensing reflectance, to [Chl] concentration [13]. The angular dependence of the water-leaving radiance in Case 1 ocean waters has been taken into account by a series of theoretical studies [14–17].

Conveniently, the water-leaving radiance L_w just above the air–sea interface (denoted as 0^+) is related to the downwelling irradiance E_d through Eq. (1) [17]

$$L_w(0^+,\theta_s,\theta,\phi,\lambda,W,\mathrm{IOP}) = E_d(0^+,\theta_s,\lambda)\Re(\theta',W)\frac{f(\theta_s,W,\mathrm{IOP})}{Q(\theta_s,\theta',\phi,W,\mathrm{IOP})}\left(\frac{b_b}{a}\right), \quad (1)$$

where θ_s is the solar zenith angle; θ and ϕ are the viewing zenith and azimuth angles, respectively; λ is the wavelength in consideration; W is the wind speed; and θ' and θ are related through Snell's law $n_w \sin\theta' = n_a \sin\theta$, where n_w and n_a are refractive indices of the water and air, respectively. The factor f is the linear coefficient which relates the irradiance reflectance to the ratio of b_b/a, where b_b and a are the backscattering and absorption coefficients, respectively. The function Q is the ratio of upward irradiance to the in-water upward radiance. The functions L_w, E_d, f, and Q are all weakly dependent on

the atmospheric conditions like aerosol and cloud properties. These are omitted from the notation for brevity as their impacts are limited in practical scenes of ocean color satellite remote sensing. The dimensionless factor $\Re$ includes all the effects of light reflection by and transmission through the air–sea interface. The quantity $\Re$ is a function of θ', W, and θ_s, which nevertheless does not depend on the IOPs of ocean waters. The quantity $\Re$ is not explored further in this work and readers are referred to [17,18] for further information.

The IOPs of Case 1 ocean waters are primarily determined by the biological activity, which has led to correlations between the IOPs and [Chl] concentration. Parameterizations have been made based on the relations between the IOPs and [Chl] concentration, which are collectively called bio-optical models representing the average behavior of Case 1 waters. Morel *et al.* have studied the dependence of f/Q on the IOPs, θ_s, θ, ϕ, and λ in terms of a bio-optical model [17]. Ref. [17] has been validated with measurements from several field campaigns [19,20]. However, the IOP–[Chl] concentration parameterizations are not unique due to the inherent variability of the correlations. Different bio-optical models have been proposed and the IOPs predicted by these models do not necessarily agree well with each other [21]. In addition, significant deviations to the average laws have been recognized. Specifically, it is reported that the absorption coefficient of colored dissolved organic matter (CDOM) may deviate from the average bio-optical relation systematically [22]. Mobley *et al.* have pointed out that "within Case 1 waters, there is a factor-of-two (and sometimes much greater) variability in the values of optical properties for a given chlorophyll value" [23].

The IOP natural variability changes the angular distribution of the water leaving radiances. The CDOM absorption coefficient variations alter the relative importance of single and multiple scattering contributions in the total radiance field, which will in turn lead to different f/Q factors. Moreover, the impacts of the scattering coefficient variability on the f/Q factors are important because it is the scattering process which generates the water leaving radiance after all. The phase function variability is also critical as it modulates the radiance angular distribution directly. To work around the water leaving radiance angular distribution uncertainty due to the IOP natural variability, Lee *et al.* have proposed an IOP centered scheme to correct the angular distribution of the water leaving radiance [24]. Notably, the IOP centered scheme can be applied to Case 2 waters as well, which has been partially verified [20]. Nevertheless, the f/Q table of [17] is still the best option for Case 1 waters [20]. Due to its vast usage in the ocean color community, it is necessary and important to understand how the f/Q factors respond to different choices of bio-optical models and the natural variability of the IOPs.

In this paper we study the impact of the natural variabilities of the CDOM absorption and particle scattering coefficients on the angular distribution of the upwelling radiance field in ocean waters. To quantify the CDOM absorption coefficient anomaly, a constant factor Φ introduced by Morel and Gentili [25] is used [Eq. (3)]. Similar to [17], we have performed a series of radiative transfer simulations to study the ratio f/Q with the additional Φ dependence. The similarities between the f/Q values with $\Phi = 1$ and those of [17] serve an independent confirmation of the results in [17], and the differences between the two sets of data indicate the variability of f/Q due to different bio-optical model realizations. The variability of f/Q with different Φ values reveals the uncertainty of f/Q due to the CDOM absorption coefficient anomaly. Similar to the CDOM absorption coefficient case, the uncertainty of the f/Q factors resultant from the particle scattering coefficient variability is studied with a multiplication factor Φ_s ranging from 0.5 to 2.0. The differences between $\Phi_s \neq 1$ and $\Phi_s = 1$ are compared to quantify the uncertainty due to scattering coefficient variability. In addition, the f/Q uncertainty due to ocean water depolarization variability is also studied.

In the following, Section 2 covers the bio-optical model and radiative transfer methods used in this work, the results and discussion are presented in Section 3, and the conclusions are summarized in Section 4.

2. THEORETICAL AND COMPUTATIONAL METHODS

A. Bio-Optical Model

In this bio-optical model, the absorption, scattering, and backscattering coefficients of the ocean water are parameterized in terms of λ and [Chl] concentration. The scattering phase function is determined by the backscattering ratio which is the ratio of backscattering and scattering coefficients. In [17] the ocean water absorption coefficient a_t is obtained through a statistical relation between a_t and the diffuse attenuation for downward irradiance $K_d(\lambda, [\mathrm{Chl}])$, where [Chl] is the chlorophyll a concentration. The absorption coefficient from this method implicitly includes all contributions from pure sea water, phytoplankton particles, and CDOM. Differently from [17], we have adopted a method in which the contributions from different constituents have been made explicitly

$$a_t(\lambda, [\mathrm{Chl}], \Phi) = a_w(\lambda) + a_y(\lambda, [\mathrm{Chl}], \Phi) + a_p(\lambda, [\mathrm{Chl}]), \quad (2)$$

where a_t is the total absorption coefficient; and a_w, a_y, and a_p are the absorption coefficients of the pure seawater, CDOM, and phytoplankton and their covariant particles, respectively. The pure water absorption coefficient a_w is from the tabulated experimental data by Pope and Fry [26]. The CDOM absorption coefficient a_y takes the following form [25]

$$\begin{aligned} a_y(440, [\mathrm{Chl}], \Phi) &= \Phi 0.0316[\mathrm{Chl}]^{0.63} \\ a_y(\lambda, [\mathrm{Chl}], \Phi) &= a_y(440, [\mathrm{Chl}], \Phi) \\ &\quad \times \exp(-0.014(\lambda - 440)), \end{aligned} \quad (3)$$

where Φ is the dimensionless factor to quantify the CDOM absorption coefficient anomaly, and λ is the wavelength (nm). Notably $\Phi = 1$ represents the average behavior of the CDOM absorption coefficient in Case 1 waters. It is known that the direct method of Eq. (2) provides absorption coefficient close to the method of retrieving a_t from K_d [21]. The range of Φ values are from 0.1 to 10 which should cover most realistic situations. The phytoplankton particle term is

$$a_p(\lambda, [\mathrm{Chl}]) = A_p(\lambda)[\mathrm{Chl}]^{E_p(\lambda)}, \quad (4)$$

where the coefficients A_p and E_p were provided by Bricaud [27].

We assume the scattering coefficient of the CDOM is negligible. The total scattering coefficient b_t is then the sum of two terms

$$b_t(\lambda,[\mathrm{Chl}]) = b_w(\lambda) + b_p(\lambda,[\mathrm{Chl}]). \quad (5)$$

The pure seawater scattering coefficient b_w is consistent with [17] as per [28,29]

$$b_w(\lambda) = 0.00193 \cdot (550/\lambda)^{4.32}. \quad (6)$$

The symbol b_p is the scattering coefficient of phytoplankton and their covariant particles. There are quite a few choices for b_p in the literature [21,30–32]. In this work we use b_p as in [21,32]

$$b_p(\lambda,[\mathrm{Chl}]) = b_p(660,[\mathrm{Chl}])\left(\frac{\lambda}{660}\right)^{\nu}, \quad (7)$$

where $\nu = 0$ if $[\mathrm{Chl}] > 2\ \mathrm{mg\,m^{-3}}$; otherwise

$$\nu = 0.5(\log_{10}[\mathrm{Chl}] - 0.3), \quad (8)$$

if $0.02 < [\mathrm{Chl}] < 2\ \mathrm{mg\,m^{-3}}$.

The scattering coefficient at 660 nm $b_p(660)$ is parameterized as

$$b_p(660,[\mathrm{Chl}]) = \Phi_s 0.347[\mathrm{Chl}]^{0.766}, \quad (9)$$

where Φ_s is a multiplication factor in a spirit similar to Eq. (3). In this work Φ_s varies from 0.5 to 2.0, consistent with the statement by Mobley *et al.* [23]. If $\Phi_s = 1$, Eqs. (7) and (9) correspond to the average Case 1 water behavior. At $\lambda = 550$ nm and for $\Phi_s = 1$ Eqs. (7) and (9) predict $b_p(550,[\mathrm{Chl}]) = 0.3566[\mathrm{Chl}]^{0.766}$, which is however inconsistent with [17] {Eq. (8) of [17], $b_p(550,[\mathrm{Chl}]) = 0.416[\mathrm{Chl}]^{0.766}$}. We found that the coefficient of 0.416 was derived from Eq. (7) by assuming $\nu = -1$ in [21]. However, the spectral power ν is generally not equal to −1 [Eq. (8)]. Note that the same ν of Eq. (8) has also been used in [17] {Eq. (14) in [17]}, which cannot regenerate 0.347 in Eq. (9) from 0.416. In a recent work Chowdhary *et al.* have adopted the same scheme [33]. The numbers suggest that the scattering coefficients in Eq. (7) in this work are smaller than those in [17] systematically. This has caused our reflectance data to be smaller than those in [17] in general. The difference is larger if [Chl] concentration is larger. We will discuss this in greater detail in a subsequent section.

The backscattering coefficients b_{bp} is [32]

$$b_{bp}(\lambda,[\mathrm{Chl}]) = b_p(\lambda,[\mathrm{Chl}]) \cdot B_{bp}([\mathrm{Chl}]), \quad (10)$$

where the backscattering fraction B_{bp} is assumed to be spectrally neutral [32]

$$B_{bp}([\mathrm{Chl}]) = 0.002 + 0.01(0.5 - 0.25\log_{10}[\mathrm{Chl}]). \quad (11)$$

The scattering phase function of the phytoplankton particle $F_p(\Theta)$ is chosen to be the Fournier–Forand function, where Θ denotes the scattering angle [34,35]. The algorithm in [36] is adopted to determine $F_p(\Theta)$ conveniently by one parameter $B_{bp}([\mathrm{Chl}])$, which is provided by Eq. (11). In [17] the particle scattering function was based on randomly oriented spheroidal particles calculated by the T-matrix method [37]. In the end the backscattering fraction in [17] was made consistent with Eq. (11). These different choices of scattering function may lead to differences in the bidirectional reflectance, especially for the cases with small single scattering albedos where single scattering contribution prevails. In the multiple scattering region the bidirectional reflectance is insensitive to small changes in the scattering function. The impacts of phase function to the f/Q factors are not considered in this work because it is difficult to systematically quantify the phase function variations. Mobley *et al.* have studied the phase function effects using a few selected ocean water phase functions [36]. The main focus of [36] was the in-water radiation field as a function of in-water depth and the angular distribution was not studied. It is certainly important to extend our uncertainty study to the impacts of phase function variations in a future work.

B. Radiative Transfer Simulations

The radiative transfer simulations are carried out by the successive order of scattering (SOS) code for coupled atmosphere and ocean systems [38,39]. Polarization has been fully taken into account to calculate the four Stokes parameters. The air–sea interface is rough with its wave slope distribution correlated to the wind speed [40]. Three wind speeds are selected for the simulations: 0, 5, and 10 m/s. The simulations confirm that f/Q only weakly depends on wind speeds. Hereafter only the results calculated with the wind speed of zero will be presented. The spectral dependence of the ocean water refractive index is accounted for by the empirical equation in [41].

The ocean water is assumed to be homogenous and optically thick (ocean optical depth is equal to 20). The ocean bottom is black (no reflection). The ocean single scattering albedo is determined by $\omega = b_t/(a_t + b_t)$, where a_t and b_t are calculated from Eqs. (2) and (5), respectively. The ocean water scattering phase function F_t is

$$F_t(\Theta) = \frac{b_w F_w(\Theta) + b_p F_p(\Theta)}{b_t}, \quad (12)$$

where F_w is the scattering function of pure seawater [28,29].

The full 4×4 Mueller matrix information is needed in a vector radiative transfer calculation. Voss and Fry have measured the Mueller matrix for a number of ocean water samples [42]. Kokhanovsky [43] has parameterized the average reduced Mueller matrix measured by Voss and Fry [42] in terms of a few parameters including the degree of polarization $p(90°)$ at the scattering angle of 90°. The parameterization by Kokhanovsky [43] is used in this work with all the parameters fixed except that $p(90°)$ is set to vary from 0.5 to 0.8 to cover possible realistic scenes [43]. The purpose is to study the sensitivity of f/Q to different ocean water polarization properties. We found that f/Q only weakly depends on $p(90°)$, which is reasonable because ocean water polarization properties only affect the total radiances secondarily. However, it is expected that the Stokes parameters other than radiance should be greatly sensitive to $p(90°)$, which is out of scope of this work.

The atmosphere is a mixture of molecules and aerosols. The molecular scattering is conservative with no trace gas absorption considered. The molecular scattering matrix is the Rayleigh scattering matrix [44] with a depolarization of 0.0284 [45]. The vertical profile of the molecular number density is determined from the pressure and temperature profile in the 1976 U.S. standard atmosphere [46]. The column molecular

scattering optical depth is calculated with the method in [45]. The aerosol model is the maritime aerosol developed by Shettle and Fenn [47] with a relative humidity of 80%. The aerosol optical depth at 550 nm is 0.2. The altitude distribution of aerosols is based on the average distribution reported in [48]. The atmosphere is divided into 30 layers with the altitude grid determined by the "Lidar Data Altitude" field in the CALIOP L1B data product [49]. For each layer, the molecular and aerosol scattering optical depths are calculated based on the number density altitude profiles described previously. Then the scattering matrix for each layer is determined by the average of Rayleigh and aerosol scattering matrix weighted by their scattering optical depths. The single scattering albedo is found by the ratio of the total scattering to extinction optical depths for each layer.

We have used parameters identical to [17] to carry out the radiative transfer calculations. Moreover, we have three additional free parameters Φ, Φ_s, and $p(90°)$. For clarity, the complete entries are listed next

- Wavelength, λ (seven values): 412.5, 442.5, 490, 510, 560, 620, and 660 nm;
- Chlorophyll a concentration (six values): 0.03, 0.1, 0.3, 1.0, 3.0, and 10.0 mg m^{-3};
- CDOM absorption factor, Φ (five values): 0.1, 0.5, 1.0, 2.0, and 10.;
- Scattering coefficient factor, Φ_s (three values): 0.5, 1.0, and 2.0;
- Ocean water polarization at 90°, $p(90°)$ (five values): 0.5, 0.6, 0.66, 0.7, and 0.8;
- Solar zenith angle, θ_s (six values): 0°, 15°, 30°, 45°, 60°, and 75°;
- Viewing azimuth angle, ϕ (13 values): 0°–180° with increment of 15°;
- Viewing zenith angle, θ (17 values): 1.078°, 3.411°, 6.289°, 9.278°, 12.300°, 15.330°, 18.370°, 21.410°, 24.450°, 27.500°, 30.540°, 33.590°, 36.640°, 39.690°, 42.730°, 45.780°, and 48.830°.

Note that $p(90°) = 0.66$ is the value corresponding to the original measurement average by Voss and Fry [42]. The number of the f factors is $7 \times 6 \times 5 \times 3 \times 5 \times 6 = 18,900$, and that of Q is $18,900 \times 13 \times 17 = 4,176,900$. If we only use $\Phi = 1$, $\Phi_s = 1$ and $p(90°) = 0.66$, the f and Q factors reduce to those cases in [17]. We will only study f/Q below because f and Q always appear together in Eq. (1).

The Raman scattering is not included in this work. Reference [17] has shown that the Raman scattering affects the f values for waters with low chlorophyll a content ([Chl] < 0.1 mg m^{-3} from 5% (blue wavelengths) to 15% (red wavelengths). Its impacts on the Q values are not significant. With this information, we can estimate that the Raman effects on the ratio f/Q will be at most 15% in the worst case. This will not affect our overall uncertainty study in this paper. Consistently, we will compare our results with the distribution of [17] without Raman scattering included. The main differences between our simulations and those in MAG2002 are

1. The phytoplankton scattering coefficient Eq. (7) is systematically smaller than that in [17],
2. The variabilities of the CDOM absorption and particle scattering coefficients are explicitly taken into account,
3. Our calculation is based on the vector radiative transfer code,
4. A different oceanic particle volume scattering (Fournier–Forand) function is used.

3. RESULTS AND DISCUSSION

A. Comparison with the Literature

In this section we compare our results with those from [17] in order to achieve two purposes

- Cross check our simulations with existing data in the literature to confirm its validity,
- Assess the uncertainty of the f/Q factors due to the underlying assumptions in the theoretical model.

The comparison is made via the relative percentage difference of f/Q

$$\zeta = 100\% \cdot \frac{f/Q_{\Phi=\Phi_s=1} - f/Q_{\mathrm{MAG2002}}}{f/Q_{\mathrm{MAG2002}}}, \tag{13}$$

where the quantity $f/Q_{\Phi=\Phi_s=1}$ is the f/Q factor calculated by the model presented in this work with $\Phi = \Phi_s = 1$, and the f/Q_{MAG2002} value refers to [17] with Raman effects excluded. Figure 1 shows the histogram of ζ for all 278,460 cases with $\Phi = \Phi_s = 1$. The most frequent value of ζ is around −1% which is quite small considering all the different assumptions used between the two studies. The overall negative values of ζ are explainable due to the fact that our scattering coefficients are systematically smaller than those in [17].

The ζ values should be more negative as the chlorophyll a concentration values increase because the differences in b_p are larger for larger chlorophyll a concentration values. Figures 2(a)–2(d) show the distribution of ζ as a function of viewing zenith and azimuth angles for selected wavelengths (412.5 and 560 nm) and chlorophyll a concentrations (0.1 and 10 mg m^{-3}). In Fig. 2, the ζ values, indicated by the gray scale color, are drawn in the polar coordinate system with the viewing zenith and azimuth angles indicated by the radial and angular coordinates, respectively. The viewing zenith angle scales are shown by the bold numbers along the horizontal radius, whereas the viewing azimuth angle scales are given by the numbers along the outmost semicircle. The origin of the polar coordinate system represents the upward viewing direction with the zenith angle of zero. It is clear that Figs. 2(a)–2(d) confirm

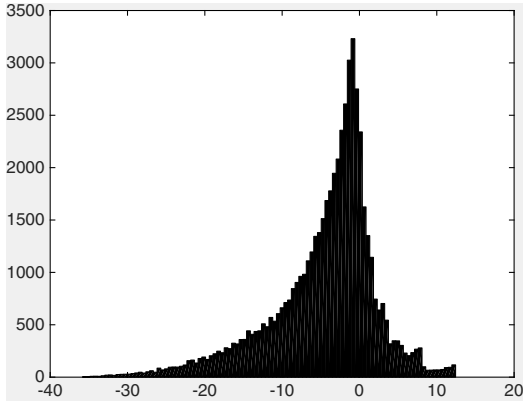

Fig. 1. Histogram of ζ.

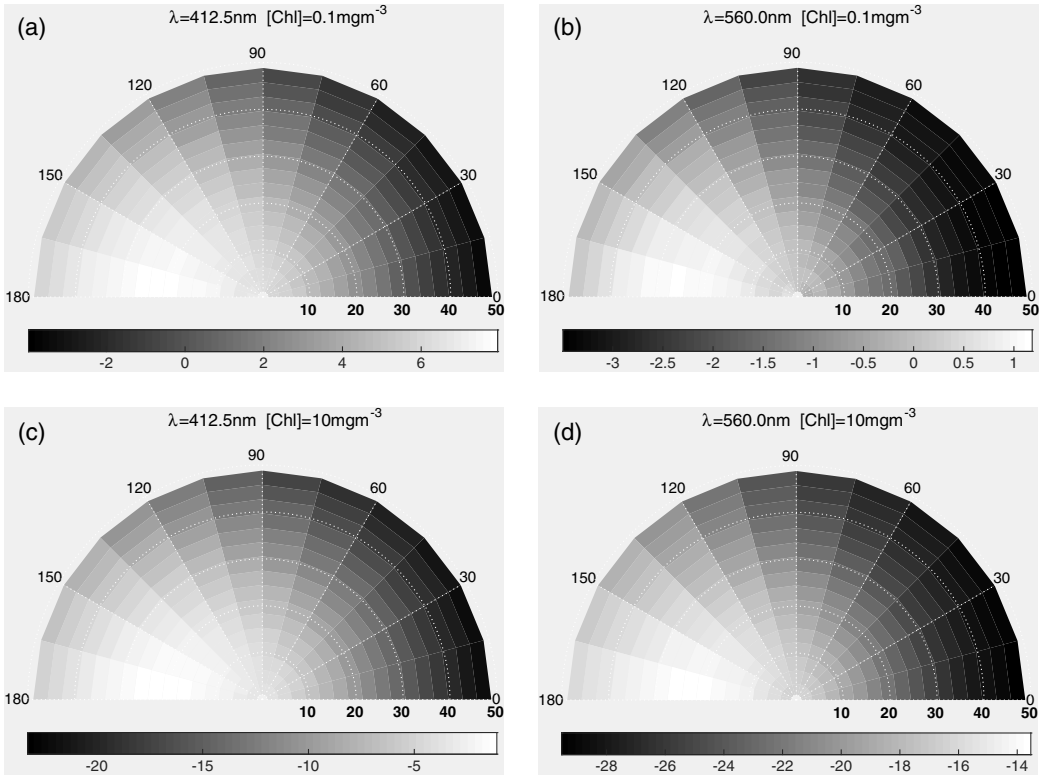

Fig. 2. Angular distribution of ζ as a function of the viewing zenith and azimuth angles for selected λ and chlorophyll a concentration. Solar zenith angle is 30°.

our expectations of how the ζ values change with chlorophyll a concentration. Moreover, ζ is closer to zero as wavelength decreases because pure water scattering becomes more dominant in shorter wavelengths, and the pure water scattering is the same for both [17] and this work.

Recall that the solar zenith angle in Fig. 2 is 30° so that the backscattering direction for the direct solar light transmitted through the air–sea interface has the zenith angle of $\arcsin(\sin(30°)/1.34) \approx 21°$, where 1.34 is the nominal value of water refractive index. With this notion it is observed that the signed ζ value is always largest at the backscattering direction. In other words the signed ζ value is smallest in the more forward scattering direction (viewing azimuth angle around 0°). This pattern is most probably due to the different scattering functions used in the simulation (the Fournier–Forand function versus calculations based on the T-matrix method). As it is seen from Fig. 1, $|\zeta|$ can be as large as 30%–40%. In order to confirm these large differences are physical, we selected a few cases with the largest $|\zeta|$ and recalculate the bidirectional reflectance factors of f/Q based on the Monte Carlo method [50], an independent vector radiative transfer solver, using the same inherent optical properties for the atmosphere and ocean systems. The f/Q factors agree well for those cases between the Monte Carlo and SOS methods (relative differences smaller than 1%). This means that the large differences in Fig. 1 are physical and they come from the bio-optical model and IOP differences.

Although some large differences are shown in Fig. 1, the two sets of data agree pretty well in the statistical sense. First, the most frequent values of ζ is very close to zero (−1%). Second, the standard deviation σ of the distribution in Fig. 1 is rather small (6.84%), and the ζ values for around 81% of the cases are smaller than 10%. Given the facts listed previously, we believe both goals listed at the beginning of this section are achieved and the 1 σ value of 6.84% could be regarded as the uncertainty of the theoretical f/Q values, due to different assumptions made on the IOPs.

B. Uncertainty due to the CDOM Absorption Coefficient Anomaly

Another purpose of this work is to study the variation of f/Q due to the CDOM absorption coefficient anomaly. Similar to Eq. (13), the quantity ζ' is introduced

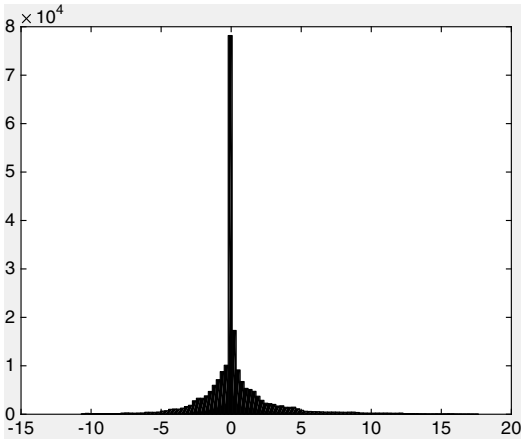

Fig. 3. Histogram of ζ'.

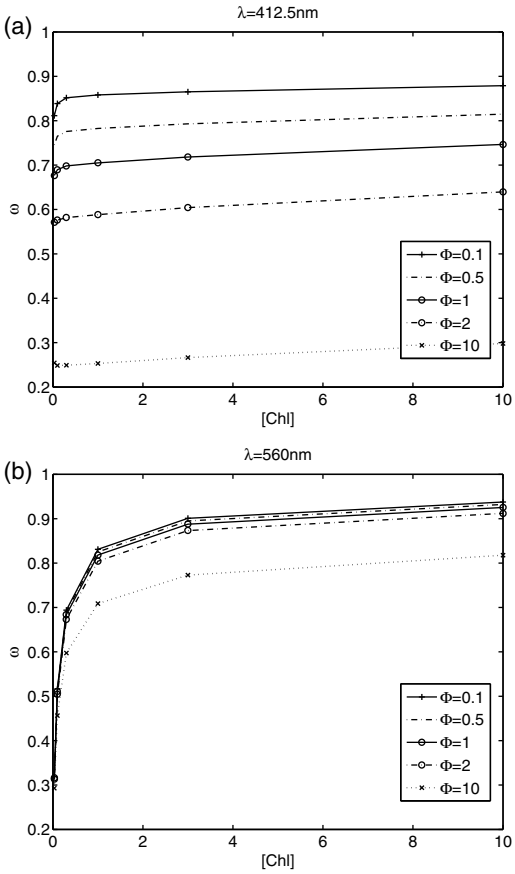

Fig. 4. Single scattering albedo of ocean water.

$$\zeta' = 100\% \cdot \frac{f/Q_{\Phi\neq 1,\Phi_s=1} - f/Q_{\Phi=1,\Phi_s=1}}{f/Q_{\Phi=1,\Phi_s=1}}. \quad (14)$$

Figure 3 shows the histogram of ζ' for all the cases with $\Phi \neq 1$, and $\Phi_s = 1$. The ζ' distribution is much narrower than that of the ζ values with the peak location roughly at zero. The standard deviation of the ζ' distribution in Fig. 3 is 2.60%, and the $|\zeta'|$ values for 93% of the cases studied are smaller than 5%.

To gain more insight on the physics behind the distribution of ζ', Figs. 4(a) and 4(b) show the single scattering albedos ω for the wavelength of 412.5 and 560 nm. The Φ values affect the ω values more for smaller wavelengths. Consequently, the impacts of the CDOM absorption coefficient anomaly are larger for shorter wavelengths. Figure 5 shows the ζ' value as a function of the viewing angles, which are plotted in a way similar to Fig. 2. The chlorophyll a concentration value is [Chl] = 0.3 mg m^{-3}. The ζ' values range from −3% to 5% at $\lambda = 412.5$ nm, and from −0.3% to 2% at $\lambda = 560$ nm. This is consistent with the effects of Φ on ω shown in Fig. 4. Moreover, the CDOM absorption decreases exponentially as wavelength increases as suggested by Eq. (3). Overall this leads to smaller impacts of the Φ values for longer wavelengths in the ocean water reflectance model.

C. Uncertainty due to Particle Scattering Coefficient Anomaly

To study the f/Q uncertainty due to scattering coefficient variation, we define the error ζ'' in the following

$$\zeta'' = 100\% \cdot \frac{f/Q_{\Phi=1,\Phi_s\neq 1} - f/Q_{\Phi=1,\Phi_s=1}}{f/Q_{\Phi=1,\Phi_s=1}}. \quad (15)$$

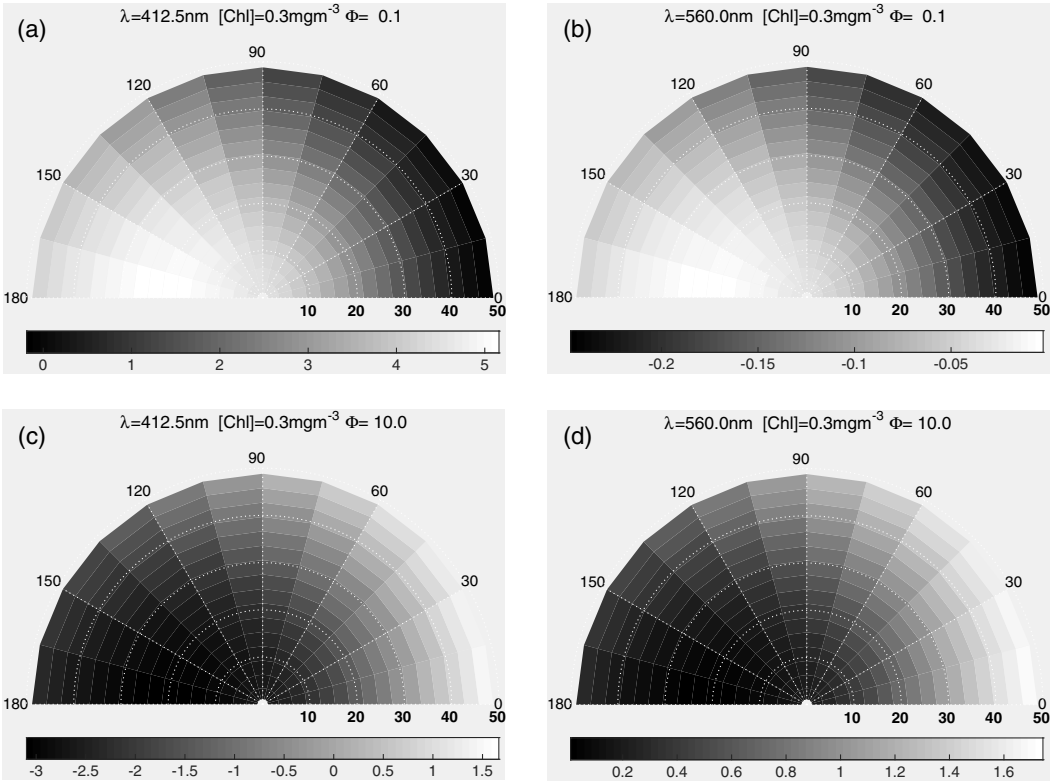

Fig. 5. ζ' as a function of viewing zenith and azimuth angles for selected λ and Φ.

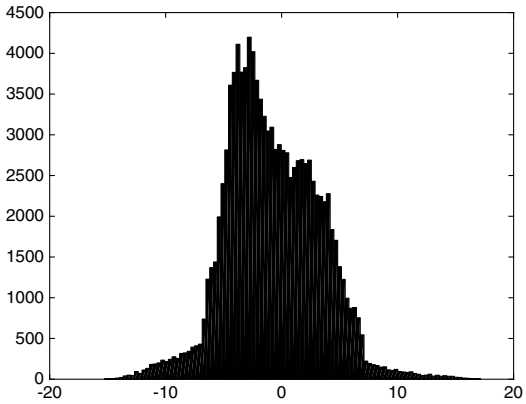

Fig. 6. Histogram of ζ''.

Figure 6 shows the histogram of ζ''. The standard deviation of ζ'' is 4.02%. The $|\zeta''|$ values are smaller than 5% for 81% of the total cases studied. Figures 7(a)–7(d) show the distribution of ζ'' as a function of viewing angles at 412.5 and 560 nm and for $\Phi_s = 0.5$ and $\Phi_s = 2.0$. As expected, ζ'' is mostly negative for $\Phi_s = 0.5$, and it is mostly positive for $\Phi_s = 2.0$, although there are still some negative values around the edge of the viewing cone in the forward principle plane. What is interesting is that ζ'' is mostly negative in the backscattering region and for smaller scattering coefficients ($\Phi_s = 0.5$). There is a small forward region where ζ'' is larger than zero. This pattern is just the opposite if the scattering coefficient is larger ($\Phi_s = 2.0$). The reason is that larger scattering coefficients increase multiple scattering contribution, which makes the radiation field less anisotropic. Oppositely, smaller scattering coefficients lead to a larger water leaving radiance around the forward principle plane $\phi_v = 0$.

Recall that we have also selected a number of $p(90°)$ values in the inputs of radiative transfer simulations. The uncertainty of f/Q due to different polarization characteristics of the ocean waters could be assessed in a way similar to the spread of ζ'. Our simulation results (data not shown) suggest that the variation of f/Q is very small due to the $p(90°)$ variations (<1%), which is understandable because the degree of polarization for water leaving radiance is generally small. Nonetheless, the polarization of the water leaving radiance may be significant under some specific conditions. One such example is when the solar zenith angle is close to Brewster's angle of the water surface. At this incident angle the transmitted solar light is completely polarized for a flat ocean surface. As a consequence, the resultant radiance reflected by the ocean water body is also strongly polarized.

4. CONCLUSIONS

We revisit the classical bidirectional reflectance properties of ocean waters with a bio-optical model. If the average CDOM absorption coefficient is considered, our results are generally smaller than those of [17]. The reason is that the scattering coefficients used in this work are systematically smaller than those used in [17]. The relative difference Eq. (13) has a most frequent value of −1%, and the 1 σ standard deviation of the distribution of ζ is 6.84%. The ζ values for 81% of the total

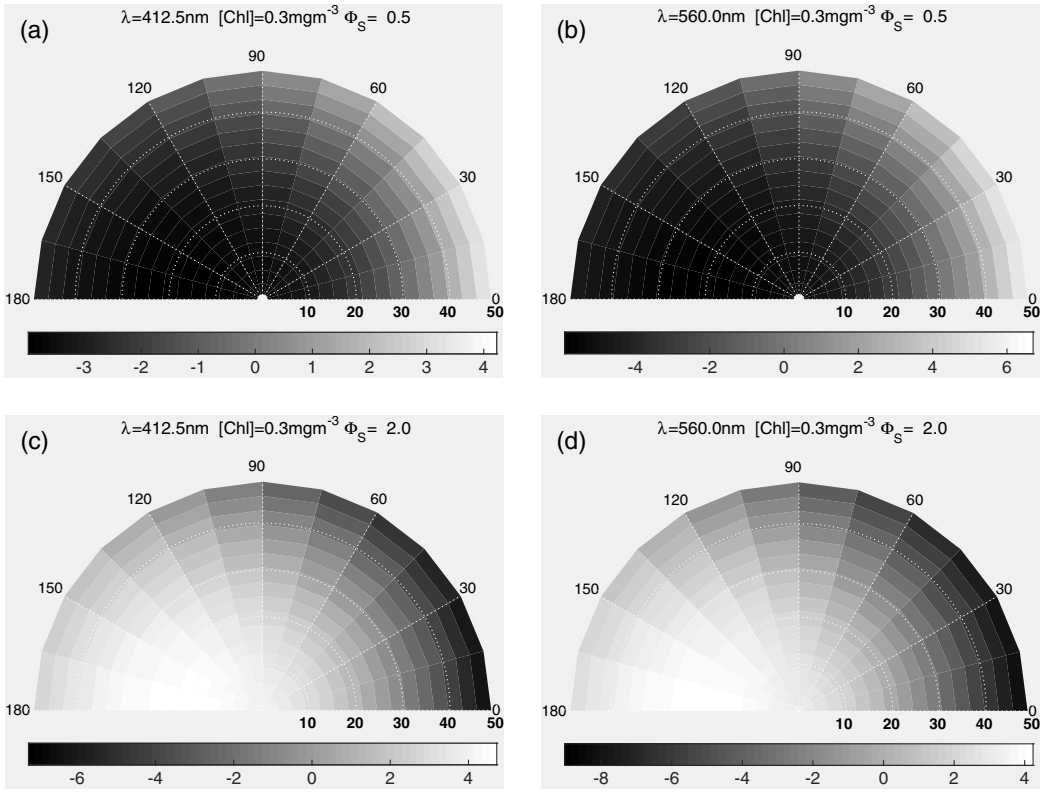

Fig. 7. ζ'' as a function of viewing zenith and azimuth angles for selected λ and Φ_S.

cases are smaller than 10%. The difference observed in this work can be regarded as the general uncertainty of the bidirectional correction of the water leaving radiance due to different inherent optical property assumptions. The uncertainty of f/Q due to the CDOM absorption coefficient is studied by adjusting a constant factor Φ [Eq. (3)]. It is shown that the 1 σ standard deviation of the f/Q variations due to the CDOM absorption coefficient anomaly is 2.60%. The variations of f/Q due to the CDOM absorption coefficient are smaller than 5% for 93% of the cases studied. The uncertainty of f/Q due to the hydrosol scattering coefficient variation is studied by using a factor $0.2 < \Phi_s < 2.0$. The 1 σ standard deviation of the f/Q variations due to the particle scattering is 4.02%, and for 81% of the cases the variations of f/Q are smaller than 5%. We have also found that the f/Q variation due to the ocean water polarization properties is negligibly small. This work helps to estimate the uncertainty of ocean color remote sensing algorithms which utilize the f/Q values distributed by [17].

This work was supported by the NASA Radiation Science Program administrated by Hal Maring and the Biogeochemistry Program administrated by Paula Bontempi. We appreciate the three anonymous reviewers for their constructive comments.

REFERENCES

1. C. R. McClain, "A decade of satellite ocean color observations," Ann. Rev. Marine Sci. **1**, 19–42 (2009).
2. J.-M. André and A. Morel, "Atmospheric corrections and interpretation of marine radiances in CZCS imagery," Oceanologica Acta **14**, 3–22 (1991).
3. M. Wang and H. R. Gordon, "A simple, moderately accurate, atmospheric correction algorithm for SeaWiFS," Rem. Sens. Environ. **50**, 231–239 (1994).
4. K. Ding and H. R. Gordon, "Atmospheric correction of ocean-color sensors–Effects of the Earth's curvature," Appl. Opt. **33**, 7096–7106 (1994).
5. H. R. Gordon and M. Wang, "Influence of oceanic whitecaps on atmospheric correction of ocean-color sensors," Appl. Opt. **33**, 7754–7763 (1994).
6. H. R. Gordon, "Atmospheric correction of ocean color imagery in the Earth Observing System era," J. Geophys. Res. **102**, 17081–17106 (1997).
7. D. K. Clark, H. R. Gordon, K. J. Voss, Y. Ge, W. W. Broenkow, and C. Trees, "Validation of atmospheric correction over the oceans," J. Geophys. Res. **102**, 17209–17217 (1997).
8. D. Antoine and A. Morel, "A multiple scattering algorithm for atmospheric correction of remotely-sensed ocean colour (MERIS instrument): principle and implementation for atmospheres carrying various aerosols including absorbing ones," Int. J. Remote Sens. **20**, 1875–1916 (1999).
9. C. Hu, K. L. Carder, and F. E. Muller-Karger, "Atmospheric correction of SeaWiFS imagery over turbid coastal waters: a practical method," Remote Sens. Environ. **74**, 195–206 (2000).
10. C. Hu, K. L. Carder, and F. E. Muller-Karger, "Atmospheric correction of SeaWiFS imagery: assessment of the use of alternative bands," Appl. Opt. **39**, 3573–3581 (2000).
11. D. A. Siegel, M. H. Wang, S. Maritorena, and W. Robinson, "Atmospheric correction of satellite ocean color imagery: the black pixel assumption," Appl. Opt. **39**, 3582–3591 (2000).
12. B. Yan, K. Stamnes, W. Li, B. Chen, J. J. Stamnes, and S. C. Tsay, "Pitfalls in atmospheric correction of ocean color imagery: how should aerosol optical properties be computed?" Appl. Opt. **41**, 412–423 (2002).
13. H. R. Gordon and K. J. Voss, "MODIS normalized water-leaving radiance algorithm theoretical basis document (MOD 18)," Version 5, May 2004, http://modis.gsfc.nasa.gov/data/atbd/atbd_mod18.pdf.
14. A. Morel and B. Gentili, "Diffuse reflectance of oceanic waters: its dependence on Sun angle as influenced by the molecular scattering contribution," Appl. Opt. **30**, 4427–4438 (1991).
15. A. Morel and B. Gentili, "Diffuse reflectance of oceanic waters. II. Bidirectional aspects," Appl. Opt. **32**, 6864–6879 (1993).
16. A. Morel and B. Gentili, "Diffuse reflectance of oceanic waters. III. Implication of bidirectionality for the remote-sensing problem," Appl. Opt. **35**, 4850–4862 (1996).
17. A. Morel, D. Antoine, and B. Gentili, "Bidirectional reflectance of oceanic waters: accounting for Raman emission and varying particle scattering phase function," Appl. Opt. **41**, 6289–6306 (2002).
18. H. R. Gordon, "Normalized water-leaving radiance: revisiting the influence of surface roughness," Appl. Opt. **44**, 241–248 (2005).
19. K. J. Voss, A. Morel, and D. Antoine, "Detailed validation of the bidirectional effect in various Case 1 waters for application to ocean color imagery," Biogeosciences **4**, 781–789 (2007).
20. A. C. R. Gleason, K. J. Voss, H. R. Gordon, M. Twardowski, J. Sullivan, C. Trees, A. Weidemann, J.-F. Berthon, D. Clark, and Z.-P. Lee, "Detailed validation of the bidirectional effect in various Case I and Case II waters," Opt. Express **20**, 7630–7645 (2012).
21. A. Morel and S. Maritorena, "Bio-optical properties of oceanic waters: a reappraisal," J. Geophys. Res. **106**, 7163–7180 (2001).
22. A. Morel, H. Claustre, D. Antoine, and B. Gentili, "Natural variability of bio-optical properties in Case 1 waters: attenuation and reflectance within the visible and near-UV spectral domains as observed in South Pacific and Mediterranean waters," Biogeosciences **4**, 2147–2178 (2007).
23. C. D. Mobley, D. Stramski, W. P. Bissett, and E. Boss, "Optical modeling of ocean waters: is the Case 1–Case 2 classification still useful?" Oceanography **17**, 60–67 (2004).
24. Z. P. Lee, K. Du, K. J. Voss, G. Zibordi, B. Lubac, R. Arnone, and A. Weidemann, "An inherent-optical-property-centered approach to correct the angular effects in water-leaving radiance," Appl. Opt. **50**, 3155–3167 (2011).
25. A. Morel and B. Gentili, "A simple band ratio technique to quantify the colored dissolved and detrital organic material from ocean color remotely sensed data," Rem. Sens. Environ. **113**, 998–1011 (2009).
26. R. M. Pope and E. S. Fry, "Absorption spectrum (380–700 nm) of pure water. II Integrating measurements," Appl. Opt. **36**, 8710–8723 (1997).
27. A. Bricaud, A. Morel, M. Babin, K. Allali, and H. Claustre, "Variations of light absorption by suspended particles with chlorophyll a concentration in oceanic (case 1) waters: analysis and implications for bio-optical models," J. Geophys. Res. **103**, 31033–31044 (1998).
28. A. Morel, "Optical properties of pure water and pure sea water," in *Optical Aspects of Oceanography*, N. G. Jerlov and E. S. Nielsen, eds. (Academic, 1974), pp. 1–24.
29. C. D. Mobley, *Light and Water: Radiative Transfer in Natural Waters* (Academic, 1994).
30. H. R. Gordon and A. Morel, *Remote assessment of ocean color for interpretation of satellite visible imagery: A review* (Springer, 1983).
31. K. Zhang, W. Li, H. Eide, and K. Stamnes, "A bio-optical model suitable for use in forward and inverse coupled atmosphere ocean radiative transfer models," J. Quant. Spectrosc. Radiat. Transfer **103**, 411–423 (2007).
32. Y. Huot, A. Morel, M. S. Twardowski, D. Stramski, and R. A. Reynolds, "Particle optical backscattering along a chlorophyll gradient in the upper layer of the eastern South Pacific Ocean," Biogeosciences **5**, 495–507 (2008).
33. J. Chowdhary, B. Cairns, F. Waquet, K. Knobelspiesse, M. Ottaviani, J. Redemann, L. Travis, and M. I. Mishchenko, "Sensitivity of multiangle, multispectral polarimetric remote sensing over open oceans to water-leaving radiance: analyses of RSP data acquired during the MILAGRO campaign," Rem. Sens. Environ. **118**, 284–308 (2012).
34. G. Fourier and J. L. Forand, "Analytic phase function for ocean water," Proc. SPIE **2258**, 194–201 (1994).
35. G. Fournier and M. Jonasz, "Computer-based underwater imaging analysis," Proc. SPIE **3761**, 62–70 (1999).

36. C. D. Mobley, L. K. Sundman, and E. Boss, "Phase function effects on oceanic light fields," Appl. Opt. **41**, 1035–1050 (2002).
37. M. I. Mishchenko, L. D. Travis, and D. W. Mackowski, "T-matrix computations of light scattering by nonspherical particles: a review," J. Quant. Spectrosc. Radiat. Transfer **55**, 535–575 (1996).
38. P. Zhai, Y. Hu, C. R. Trepte, and P. L. Lucker, "A vector radiative transfer model for coupled atmosphere and ocean systems based on successive order of scattering method," Opt. Express **17**, 2057–2079 (2009).
39. P. Zhai, Y. Hu, J. Chowdhary, C. R. Trepte, P. L. Lucker, and D. B. Josset, "A vector radiative transfer model for coupled atmosphere and ocean systems with a rough interface," J. Quant. Spectrosc. Radiat. Transfer **111**, 1025–1040 (2010).
40. C. Cox and W. Munk, "Measurement of the roughness of the sea surface from photographs of the suns glitter," J. Opt. Soc. Am. **44**, 838–850 (1954).
41. X. Quan and E. S. Fry, "Empirical equation for the index of refraction of seawater," Appl. Opt. **34**, 3477–3480 (1995).
42. K. J. Voss and E. S. Fry, "Measurement of the Mueller matrix for ocean water," Appl. Opt. **23**, 4427–4439 (1984).
43. A. A. Kokhanovsky, "Parameterization of the Mueller matrix of oceanic waters," J. Geophys. Res. **108**, 3175 (2003).
44. J. E. Hansen and L. D. Travis, "Light scattering in planetary atmospheres," Space Sci. Rev. **16**, 527–610 (1974).
45. C. Tomasi, V. Vitale, B. Petkov, A. Lupi, and A. Cacciari, "Improved algorithm for calculations of Rayleigh-scattering optical depth in standard atmospheres," Appl. Opt. **44**, 3320–3341 (2005).
46. Committee on Extension to the Standard Atmosphere, *U. S. Standard Atmosphere* (U.S. Government Printing Office, 1976).
47. E. P. Shettle and R. W. Fenn, "Models for the aerosols of the lower atmosphere and the effects of humidity variations on their optical properties," Rep. AFGL-TR-79-0214 (U.S. Air Force Geophysics Laboratory, 1979).
48. N. Braslau and J. V. Dave, "Effect of aerosols on the transfer of solar energy through realistic model atmospheres. Part I: Non-absorbing aerosols," J. Appl. Meteor. **12**, 601–615 (1973).
49. C. A. Hostetler, Z. Liu, J. Reagan, M. Vaughan, D. Winker, M. Osborn, W. H. Hunt, K. A. Powell, and C. R. Trepte, "CALIOP algorithm theoretical basis document: calibration and level 1 data products," PC-SCI-201, Release 1.0, 2006.
50. P. Zhai, G. W. Kattawar, and P. Yang, "Impulse response solution to the three-dimensional vector radiative transfer equation in atmosphere-ocean systems. I. Monte Carlo method," Appl. Opt. **47**, 1037–1047 (2008).